

1 **An assessment of Arctic Ocean freshwater content changes from**
2 **the 1990s to the 2006 – 2008 period**

3 **Benjamin Rabe^{a*}, Michael Karcher^a, Ursula Schauer^a, John M.**
4 **Toole^b, Richard A. Krishfield^b, Sergey Pisarev^c, Frank Kauker^{a*},**
5 **Rüdiger Gerdes^a, Takashi Kikuchi^d**

6 ^a *Alfred Wegener Institute for Polar and Marine Research, Germany*

7 ^b *Woods Hole Oceanographic Institution, USA*

8 ^c *Shirshov Institute of Oceanology, Russia*

9 ^d *Japan Agency for Marine-Earth Science and Technology, Japan*

10 *December, 2010*

11 *Manuscript accepted for publication in Deep-Sea Research Part I*

12 *DOI: 10.1016/j.dsr.2010.12.002*

13 *Corresponding author current address:

14 AWI for Polar and Marine Research

15 Bussestr. 24, Postfach 120161

16 27515 Bremerhaven, Germany

17 Ph: +49 (0)471 4831 2403

18 Fax: +49 471 4831 1797

19 email: Benjamin.Rabe@awi.de

Abstract

20

21 Unprecedented summer-season sampling of the Arctic Ocean during the period 2006–2008 makes
22 possible a quasi-synoptic estimate of liquid freshwater (LFW) inventories in the Arctic Ocean basins.
23 In comparison to observations from 1992 – 1999, LFW content relative to a salinity of 35 in the layer
24 from the surface to the 34 isohaline increased by $8400 \pm 2000 \text{ km}^3$ in the Arctic Ocean (water depth
25 greater than 500 m). This is close to the annual export of freshwater (liquid and solid) from the Arctic
26 Ocean reported in the literature.

27 Observations and a model simulation show regional variations in LFW were both due to changes
28 in the depth of the lower halocline, often forced by regional wind-induced Ekman pumping, and a
29 mean freshening of the water column above this depth, associated with an increased net sea ice melt
30 and advection of increased amounts of river water from the Siberian shelves. Over the whole Arctic
31 Ocean, changes in the observed mean salinity above the 34 isohaline dominated estimated changes in
32 LFW content; the contribution to LFW change by bounding isohaline depth changes was less than a
33 quarter of the salinity contribution, and non-linear effects due to both factors were negligible.

34 **Keywords:** Arctic; Freshwater; Observation; Model; IPY; Upper Ocean

1 Introduction

Liquid freshwater (LFW) plays a major role in the Arctic Ocean: the vertical stratification in the halocline between the fresh surface layer and the salty, warm Atlantic Water (e.g. *Rudels et al.*, 2004) limits the upward transfer of heat and thus influences the formation and melting of sea ice (e.g. *MacDonald*, 2000). LFW affects not only the Arctic Ocean circulation but also influences the circulation in the Atlantic, as it is exported via the Fram Strait and the passages of the Canadian Arctic Archipelago into regions of deep water formation in the Nordic Seas and the North Atlantic (*Gerdes et al.*, 2008). Model studies have shown that this LFW export influences the large scale ocean circulation, such as the Meridional Overturning Circulation (MOC; e.g. *Koenigk et al.*, 2007; *Rennermalm et al.*, 2007) and the horizontal gyres (*Brauch and Gerdes*, 2005). LFW from the Arctic thus has a direct impact on climate (*Häkkinen*, 1999; *Haak et al.*, 2003)

The LFW budget of the Arctic Ocean (*Serreze et al.*, 2006; *Dickson et al.*, 2007) consists of inputs from Eurasian and North American river runoff, the Norwegian coastal current via the Eurasian shelves, precipitation, ice melt and the inflow from the Pacific through the Bering Strait; sinks of LFW are the export through the Canadian Arctic Archipelago and the western Fram Strait, and the formation and export of sea ice. Inflow of saline Atlantic Water (AW) occurs through the eastern Fram Strait and, in modified form, via the Barents Sea. The variability of this LFW budget, for instance the storage and export of LFW in the Arctic Ocean and the Nordic Seas (e.g. *Häkkinen and Proshutinsky*, 2004), is still not fully understood. From observations, (*Curry and Mauritzen*, 2005) found that $19000 \pm 5000 \text{ km}^3$ of freshwater¹ were added to the Nordic Seas and the Subpolar North Atlantic basins between the early 1965s and the 1995. Model studies have shown two strong negative anomalies in LFW export from the Arctic between 1970 and the mid 1990s. On average, the annual LFW export, referenced to a salinity of 35, was 500 km^3 higher between 1970 and 1995 than during the second half of the 20th century, when the time-mean export was $3050 \text{ km}^3/\text{yr}$ (*Köberle and Gerdes*, 2007; *Gerdes et al.*, 2008). The increased export represents a potential loss of LFW for the Arctic Ocean of 12500 km^3 between 1970 and 1995, close to the decline in the Arctic Ocean LFW reservoir in the model experiments during this time period and comparable to the LFW gain for the Nordic Seas and the Subpolar Basins described by *Curry and Mauritzen* (2005). Subsequent to 1995, the model

¹they used the time average salinities from the 1950s in discrete layers as reference salinities to calculate the freshwater anomaly relative to that time period

63 studies show an accumulation of LFW in the Arctic Ocean and a decrease in LFW export up to 2001.
64 On the other hand, an analysis of mooring based and ship based observations estimates the export of
65 LFW from the Arctic Ocean through the western Fram Strait to be approximately constant between
66 1998 and 2008 (*de Steur et al.*, 2009).

67 During the 1990s the pathways of Pacific Water (PW) and Eurasian river water through the cen-
68 tral Arctic changed relative to the prevailing conditions during the previous 40 years (*Steele et al.*,
69 2004; *Karcher et al.*, 2006; *Newton et al.*, 2008). Model studies indicate that the changes in the hy-
70 drography and circulation in the Arctic Ocean covary with large scale sea surface pressure and wind
71 stress patterns (e.g. *Proshutinsky and Johnson*, 1997; *Dukhovskoy et al.*, 2004). *Proshutinsky et al.*
72 (2009) analyzed observations in the Beaufort Gyre, which extends over the Beaufort Sea, the south-
73 ern Canada Basin and often over parts of the Chukchi Plateau (CP; Figure 1). Their observations
74 during July/August/September (JAS) from 1950 to 2007 show pronounced decadal variability and in-
75 dicate a shift of the center of the gyre related to the large scale wind field. In an analysis based on the
76 sparse observational data available over the past 100 years, *Polyakov et al.* (2008) infer a decrease in
77 LFW in the Arctic Ocean from the mid-1960s to the mid-1990s. They attribute this to enhanced ice
78 production and increased export of LFW driven by atmospheric circulation.

79 In this study, we analyze changes between two recent decades, making use of the unprecedented
80 observational coverage during the International Polar Year (2006 – 2008) and observations over a
81 longer time period during the 1990s. The data coverage allows us, for the first time, to use objective
82 analysis to estimate not only the large scale spatial distribution of LFW and the LFW content but
83 also quantify the error associated with these estimates. We focus on LFW calculated from salinity
84 observations in the upper 500m of the whole deep Arctic Ocean bounded by the 500m isobath (Figure
85 1). Only observations during JAS are considered, as the year-round data coverage is strongly biased
86 toward these months. The results will be put in context with other observations, underlying physical
87 processes and output from a simulation with a coupled ice-ocean general circulation model, the North
88 Atlantic/Arctic Ocean Sea Ice model (NAOSIM; *Karcher et al.*, 2003).

2 Methods

2.1 Observations

Salinity (S) profile data are taken from Conductivity Temperature Depth (CTD) and Expendable CTD (XCTD) observations from ships, submarines and ice drifting stations. Since 2004, these data have been augmented by autonomous measurements (*Kikuchi et al.*, 2007; *Krishfield et al.*, 2008), which, around the time of the International Polar Year (IPY; 2007 – 2009), lead to an Arctic-wide coverage of measurements. The list of sources is given in Table 1. Despite the increasing number of observations from autonomous platforms there is a strong bias of data coverage toward Arctic summer. In order to avoid obscuring interannual variability with an unresolved seasonal cycle we use only data from JAS. Data used from the World Ocean Dataset 2009 (WOD09; *Boyer et al.*, 2009) are taken from the “CTD” part of the database (“High-resolution Conductivity-Temperature-Depth / XCTD data”, as listed in the WOD09 documentation enclosed in the dataset). The accuracy of salinity observations is around 0.01 for XCTD after calibration with ship CTD profiles (*Itoh and Shimada*, 2003; *Kikuchi*, 2008) and the same for calibrated autonomous measurements. The manufacturer’s stated accuracies for XCTD and Submerged Ship XCTD (SSXCTD) are 0.04 and 0.05, respectively. Where available, XCTD profiles that had been calibrated against conventional CTD profiles, reducing the error by a factor of two or more, were used. The accuracy of CTD casts from ships, calibrated against simultaneous water bottle samples, is generally an order of magnitude better than those of autonomous or expendable systems.

All observational data, also those taken from publicly accessible databases, were scrutinized to eliminate errors. Processing and quality control of the dataset are described in Appendix A and errors are discussed in Appendix B.

2.2 LFW calculations

To obtain a measure of LFW in the upper Arctic Ocean, the fraction of LFW content, f , relative to a reference salinity, S_{ref} (see also *Aagaard and Carmack*, 1989), was calculated between the surface and the depth of the 34 isohaline, $h = z(S = 34)$. This isohaline lies within the lower halocline, which has been shown to be largely unaltered by surface salinity throughout most of the Arctic Ocean

116 (Rudels et al., 2004). The inventory of LFW in the layer above this isohaline is given by

$$h_{fw} = \int_{z=0\ m}^{h) } f dz = \int_{z=0\ m}^h \frac{S_{ref} - S}{S_{ref}} dz, \quad (1)$$

117 where f is the fraction of LFW, S is the observed salinity and $S_{ref} = 35$, approximately the salinity of
 118 the AW inflow into the Arctic Ocean via the Fram Strait and the Barents Sea; using a reference salinity
 119 of 34.8 does not significantly change h_{fw} (see also Appendix B). River water, PW, net precipitation
 120 and ice melt are additions of LFW to the AW reference, whereas ice formation is a LFW sink. The
 121 maximum error in f due to accuracy of the salinity observations is about $2.5 \cdot 10^{-3}$. In cases where
 122 parts of the profile near the surface were not measured, the shallowest data point was used for constant
 123 extrapolation to the surface, making a mixed layer assumption. The maximum pressure of this data
 124 gap was set to 20 dbar, although most profiles have data from at least 8 dbar (the potential error of
 125 this assumption is discussed in Appendix B).

126 Different subsets of the observations were objectively mapped to obtain the horizontal distribution
 127 of h_{fw} on a regular grid. The procedure is outlined in the following section. The mapped fields of h_{fw}
 128 for the whole deep Arctic Ocean bounded by the 500 m isobath (Figure 1) were spatially integrated
 129 to obtain the LFW content between the ocean surface and h :

$$LFWC = \oint h_{fw} dA, \quad (2)$$

130 where dA is the area associated with each grid point. h_{fw} and LFWC were calculated both from the
 131 observations and from output of the NAOSIM simulation.

132 2.3 Objective mapping

133 To obtain horizontal maps of h_{fw} for selected time periods, subsets of the observations were objec-
 134 tively mapped (e.g. Bretherton et al., 1976) onto a uniform grid with 50 km distance between grid
 135 points. Our procedure is similar to that used by Böhme and Send (2005) and Böhme et al. (2008).
 136 Following McIntosh (1990), the objective estimate of a parameter O at a grid point g can be obtained
 137 from a set of observations, O_d :

$$O_g = \langle O_d \rangle + \omega \cdot (O_d - \langle O_d \rangle); \omega = C_{dg} \cdot (C_{dd} + I \cdot \langle \eta^2 \rangle)^{-1}, \quad (3)$$

138 where subscripts d and g refer to the observational (data) points and the grid points, respectively,
 139 $\langle O_d \rangle$ is the mean of O_d , calculated as in *Owens and Wong (2009)* and *Bretherton et al. (1976)*, ω
 140 is the weighting function and I is the identity matrix. The last term is the noise variance,

$$\langle \eta^2 \rangle = \frac{\sum [n][i=1](x_i - x_{ic})^2}{2n}, \quad (4)$$

141 which is the mean of the squared deviation of each individual point in O_d (i) from it's nearest neighbor
 142 in O_d (ic), in terms of the mapping scales (e.g. *Holbrook and Bindoff, 2000*). This term measures the
 143 variations between close-by data, which is different to the signal variance that measures the squared
 144 deviation of the data from the mean. C_{dg} is the data-grid covariance and C_{dd} the data-data covariance.
 145 The interpolation (mapping) uses a Gaussian covariance function containing isotropic horizontal dis-
 146 tance, D , and barotropic potential vorticity, PV (*Davis, 1998*):

$$PV = \frac{|\frac{f_d}{Z_d} - \frac{f_g}{Z_g}|}{\sqrt{\frac{f_d^2}{Z_d^2} + \frac{f_g^2}{Z_g^2}}}; D = |xy_d - xy_g|, \quad (5)$$

147 where xy is the geographic location, f the Coriolis parameter and Z the bathymetric depth, based
 148 on the International Bathymetric Chart of the Arctic Ocean (IBCAO, *Jakobsson et al., 2008*). The
 149 covariance is given by

$$C = \langle s^2 \rangle \exp\left(-\left(\frac{D^2}{L^2} + \frac{PV^2}{\Phi^2}\right)\right), \quad (6)$$

150 where the signal variance $\langle s^2 \rangle = \frac{\sum_{n=1}^{i=1} (O_d - \langle O_d \rangle)^2}{n}$, L represents the Gaussian decorrelation scale
 151 (e-folding scale) for D and Φ the scale for PV .

152 To avoid bias in the objective estimate, a reference field is often subtracted from the data before
 153 mapping. Therefore, we used Equation 4 in a two-stage procedure: First, a very smooth map of O_g
 154 was produced. Second, the residuals between each observed value and the mapped field were mapped
 155 using smaller spatial scales to give weight to the observations closest to each grid point. Finally, the
 156 mapped residuals were added to the mapped values from the first stage to obtain the horizontal map of

157 O_g . We separately mapped the observed h_{fw} and h . For the first stage mapping we used decorrelation
158 scales of $L = 600 \text{ km}$ for horizontal distance and $\Phi = 1$ to adjust the isotropic distance scale to
159 account for changes in barotropic potential vorticity, whereas the second stage used $L = 300 \text{ km}$,
160 $\Phi = 0.4$. A distance of 300 km has been shown to be the appropriate decorrelation scale for LFW
161 observations in the Canada Basin (Proshutinsky et al., 2009). Using $\Phi = 0.4$ for the non-isotropic
162 potential vorticity scaling means that a depth change from around 3000 m to 1500 m at 85° latitude
163 sets the decay scale of the Gaussian covariance, i.e. typical bathymetric changes between deep Arctic
164 basins and continental slopes or ridges. The combination of both the distance and potential vorticity
165 scales leads to non-isotropic weighting contours around each grid point. For both mapping stages,
166 only data within the large decorrelation scales from the grid point were used. If more than 60 data
167 points were available, the data were subselected: $1/3$ were randomly chosen to avoid bias toward
168 closely spaced profiles, such as from the Ice-Tethered Profilers (ITPs). The remaining $2/3$ were
169 chosen by the highest weights (ω , Equation 4), where $1/3$ lied within the small decorrelation scale
170 and $1/3$ within the large scale; note that at each grid point the covariance (and weighting) functions
171 based on the large and the small scales do not necessarily have the same shape. Observations from
172 JAS were mapped separately for the time periods 1992 – 1999 and 2006 – 2008.

173 To reduce errors in the maps of the LFW inventories, a gross range limit was used for all observed
174 LFW inventories. Furthermore, regional outliers in the observed LFW inventories, as could be caused
175 by eddies, were eliminated. For this purpose, each observed LFW inventory was compared to the
176 mean of the inventories within a 600 km radius. This mean and the standard deviation was calculated
177 from all data or, if there were more than 60 data points, from a subset selected from within the 600 km
178 and a 100 km radius in a similar way as during the mapping procedure. Each individual inventory
179 was discarded if it was more than two standard deviations away from the mean or if the difference
180 between the inventory and the mean was more than 7 m . A similar outlier elimination was applied to
181 the depth of the 34 isohaline, h , prior to mapping. Finally, 858 profiles were used for the objective
182 mapping for the time period 1992 – 1999 and 4299 for 2006 – 2008, the number for the latter period
183 being greater mainly due to the frequent sampling of the autonomous CTD systems and increased
184 observational efforts during the IPY.

185 A detailed analysis of the errors is given in Appendix B.

2.4 Numerical simulation

The numerical simulation was performed with the coupled ice-ocean model NAOSIM, which derives from the Geophysical Fluid Dynamics Laboratory modular ocean model MOM-2 (Pacanowski, 1995). The model domain contains the Arctic Ocean, the Nordic Seas and the Atlantic north of approximately 50°N. Open boundary conditions in the Atlantic and in the Bering Strait were formulated following Stevens (1991), allowing the outflow of tracers and the radiation of waves. For the Bering Strait a net volume inflow of 0.8 Sv has been applied. The initial and open boundary hydrography in January 1948 is taken from the PHC climatology (Steele et al., 2001), which is also used as a reference for a surface salinity restoring with 180 days timescale. The model is driven with daily atmospheric forcing from 1948 to 2008 (NCEP/NCAR reanalysis, Kalnay and coworkers, 1996). For a more detailed description of the model see Köberle and Gerdes (2003) and Kauker et al. (2003). In an earlier model version NAOSIM has also been used to study freshwater dynamics of the Arctic Ocean (Karcher et al., 2005; Gerdes et al., 2008; Rabe et al., 2009).

3 LFW distribution during 1992 – 1999 and 2006 – 2008

The observational maps show the maximum in the LFW inventories during JAS for both time periods in the Beaufort Sea (Figure 2). This maximum results from the persistent anticyclonic wind field, leading to Ekman pumping and a depression of the lower halocline in the Beaufort Gyre, and an accumulation of freshwater. There is a gradual decline in LFW from the Beaufort Sea toward the Siberian shelf seas and toward the Fram Strait and the Barents Sea, where AW enters the Arctic Ocean. Data coverage was overall good, except close to the Canadian Arctic Archipelago and in parts of the eastern Beaufort Sea during 1992–1999 (Figure 2a). Time averages of the simulated LFW inventories show similar large scale distributions as the mapped observations for the corresponding time periods (Figure 3). However, the extrema in the Canada and Nansen basins are weaker in the simulation, in particular during 1992 – 1999 (Figure 3a). Out of all the years under study, the simulation shows highest LFW inventories during 2008 (not shown).

A comparison of Δh_{fw} for the two periods (Figure 2c) exhibits an increase ranging from 1 to 8 m of LFW in most of the deep Arctic Ocean except the western Nansen Basin, the eastern Amundsen Basin and part of the region north of the Canadian Arctic Archipelago. For the Beaufort Sea the

214 changes hint at both a shift in the center of the Beaufort Gyre and an expansion of the gyre. In the
215 central Arctic Ocean, *Steele and Boyd* (1998) observed a salinification in the central Arctic Ocean
216 during the 1990s, resulting in a weakening of the stratification in the upper halocline. They attributed
217 this to an eastward shift of the area influenced by fresh shelf waters. *Morison et al.* (2006) extended
218 an analysis by *Steele et al.* (2004) up to 2005 to show that there is a 3 to 7 year lag in the adjustment of
219 the upper Arctic Ocean to changes in the large scale wind field, represented by the Arctic Oscillation
220 index. *Morison et al.* found that from 2000 onward, the observed hydrography of the central Arctic
221 was again getting closer to the pre-1990s state. This was also shown by *Karcher et al.* (2005) in the
222 same model simulation as used in our study. Our observations show that, regarding LFW, the trend
223 continued up to the period 2006 to 2008.

224 A comparison of the LFW changes between the two time periods based on observations (Figure
225 2c) and the simulation (Figures 3c) shows strong similarities in the large scale pattern and amplitude.
226 Regional differences are apparent, in particular in the Beaufort Sea and the southern Canada Basin,
227 where the mapped observations show a shift in the LFW maximum toward the southeast; however,
228 the lack of data north of the Canadian Arctic Archipelago during the 1990s prevents any conclusive
229 comparison in this region. Over the whole deep Arctic Ocean, the observed LFWC (equation 2) in-
230 creased by 8400 km^3 between the time periods 1992 – 1999 and 2006 – 2008. This is close to the
231 estimated total annual export of freshwater (liquid and solid) from the Arctic Ocean (*Dickson et al.*,
232 2007) and almost 20 % of the average of LFWC we observe for both time periods. In the simulation,
233 LFWC changed by 6120 km^3 , which is lower than the observational estimate, but of the same order
234 of magnitude. Nevertheless, in both the observations and the simulation we see changes in the distri-
235 bution of LFW summing up to an overall increase in LFWC. In the following section we investigate
236 possible causes of these changes.

237 4 Physical processes

238 4.1 LFW distribution

239 The LFW inventories are related to two quantities: the depth of the 34 isohaline, h , and the depth
240 averaged salinity above this isohaline, \bar{S} . In most parts of the deep Arctic Ocean, the 34 isohaline
241 is sufficiently deep, so that it is unaffected by wind-induced mixing and freezing-induced convection

242 (*Rudels et al.*, 2004). Therefore, the differences in h between 1992 – 1999 and 2006 – 2008 (Δh ,
 243 Figure 4a) are likely to be the result of Ekman Pumping (EP) due to ocean surface stress induced by
 244 wind and ice motion (e.g. *Yang*, 2006). An exception to this is the region of the boundary current
 245 carrying AW from the Fram Strait and the Barents Sea. Here the 34 isohaline is very shallow, so that
 246 even small changes in the salinity of the AW inflow as well as changes in its temperature influencing
 247 ice formation and melt (e.g. *Schauer et al.*, 2004) have an effect on the depth of this isohaline. Unlike
 248 EP, which is an adiabatic process, changes in \bar{S} ($\Delta\bar{S}$, Figure 4b) are diabatic (non-conservative),
 249 altered by changes in the salinity of advected water or local changes in sea ice melt and formation.
 250 We split the differences in h_{fw} between the two time periods into different components:

$$\Delta h_{fw} = \overbrace{\Delta h F_1}^{\text{thickness}} + \overbrace{h_1 \Delta F}^{\text{salinity}} + \overbrace{\Delta h \Delta F}^{\text{non-linear}}, \quad (7)$$

251 where $F_1 = 1 - \frac{\bar{S}_1}{S_{ref}}$, $\Delta F = -\frac{\Delta\bar{S}}{S_{ref}}$, and the subscript 1 denotes the reference values from 1992 – 1999.
 252 The three terms on the right hand side will be referred to as labeled.

253 The 34 isohaline shallowed slightly in the central and eastern Canada Basin, i.e. the northeastern
 254 part of the Beaufort Gyre, and parts of the central Arctic (Figure 4a), whereas a distinct deepening can
 255 be seen around the Chukchi Plateau and in parts of the Makarov and Eurasian basins; deepening was
 256 less pronounced in the southeastern Beaufort Gyre. The effect on changes in the LFW inventories,
 257 given by the thickness term in Equation 7 (Figure 4c), is strongest around the Chukchi Plateau. The
 258 distribution of changes in h in the simulation (Figure 5a) shows good agreement with the observations
 259 on the large scale; in particular, north of the Bering Strait, both the simulation and the observations
 260 show an increase in h (Figures 5a and 4a), with a small east-west offset in the maximum. Different
 261 tendencies can be found north of Severnaya Zemlya in the Eurasian Basin and north of Greenland,
 262 where the mapped observations indicate a sinking of the halocline, while the simulation shows a
 263 rising.

264 For a calculation of surface stress induced EP, not only the wind stress but also the effect of
 265 internal ice stress has to be taken into account. Here, we make use of the ocean surface stress from
 266 the NAOSIM ice-ocean model simulation, which is forced with daily surface winds. The ocean
 267 surface stress comprises the joint effect of wind and internal ice stresses on the oceanic motion, and
 268 the EP calculation is based on this stress. Since even in regions of predominantly downward EP,
 269 such as the Beaufort Gyre, the 34 isohaline (or any other isohaline) is not displaced downward in the

270 long term, its long-term average vertical velocity must be close to zero. The EP is counteracted by
271 processes such as deep mixing that are not analyzed here in detail. Averaged regionally and in time
272 over the whole 50 years of the simulation, the mean downward EP velocity is 0.5 cm/day in the North
273 American Basin and 1.5 cm/day in the Beaufort Gyre. A comparison of the interannual variability
274 in both regions, however, shows noticeable covariability between EP and the velocity associated with
275 the displacement of the 34 isohaline (Figure 6). Only for a brief period in the 1990s, local mixing
276 and externally driven lateral advection lead, on average, to stronger discrepancies between EP and the
277 vertical velocity of the 34 isohaline. Thus, our model simulation supports earlier studies that EP is a
278 key process for the determination of changes in h in the Beaufort Gyre (*Proshutinsky et al.*, 2009). In
279 addition, our results indicate that this holds for the entire North American Basin.

280 In much of the deep Arctic Ocean we observe a decrease in \bar{S} (Figure 4b) with values of $\Delta\bar{S}$
281 as low as -2 in the Makarov Basin and parts of the Eurasian Basin. Around the Chukchi Plateau
282 and near the edges of the Eurasian Basin \bar{S} increased. In the earlier period, h was lower in much of
283 the Eurasian Basin than in the central Arctic and the Canada Basin. Therefore, the strong decreases
284 in \bar{S} in the Eurasian Basin lead to smaller increases in the LFW inventories due to the salinity term
285 in Equation 7 (Figure 4d), than elsewhere. In the simulation the increases in \bar{S} are similar to the
286 observations north of the Bering Strait and north of the Fram Strait. The main simulated decrease is
287 found in the Canada Basin, whereas there were weaker, localized decreases in the Eurasian Basin.

288 Changes in the net sea ice melt between the two time periods may have influenced \bar{S} either locally
289 or via advection of freshwater, (salt) from ice melt (formation), for example from the shelves. From
290 the difference in simulated net sea ice melt between 2006 – 2008 and 1992 – 1999 (Figure 5c) we
291 find a freshwater input from net melt around the Chukchi Plateau. This likely contributed to the
292 decrease in salinity downstream to the east in the Beaufort Sea, evident in the maps of seen \bar{S} from
293 the observations (Figure 4b) and the simulation (Figure 5b). In much of the North American Basin,
294 on the East Siberian and Laptev sea shelves and in the basins to the north net sea ice melt increased
295 (Figure 5c), whereas in parts of the central Arctic and the Eurasian Basin small decreases occurred.

296 Although we observe an overall freshening in the Canada Basin, there was a redistribution of LFW
297 in the southern part of the Beaufort Gyre (Figure 2c), associated with both changes in Δh (Figure 4a)
298 and in \bar{S} (Figure 4b). Here, tracer measurements between 1987 and 2007 show less removal of LFW
299 within the surface layer due to a reduction in winter ice formation, whereas meteoric water (river

runoff and precipitation) was increasing in the center of the gyre (Yamamoto-Kawai et al., 2009); in 2006 and 2007, Yamamoto-Kawai et al. observed that also net ice melt increased in that part of the gyre. However, some of the observed increases in LFW near the surface were compensated by decreases in LFW contained in Pacific Water below (Proshutinsky et al., 2009). Thus both a changed Ekman pumping due to changing ocean surface stress and an accumulation of river water and ice melt in the North American Basin have contributed to the observed changes between the two time periods.

In large parts of the Eurasian Basin, along the Lomonosov Ridge and in the Makarov Basin, we find that the observed increase in LFW can be mostly attributed to a decrease in the observed \bar{S} . Here, the simulation indicates no significant or uniform change in net sea ice melt (Figure 5c). Furthermore, there are indications from four years of hydrographic observations at the Lomonosov Ridge close to the North Pole since 1990 that ice melt water was not at an extreme high in 2007 (Bert Rudels pers. comm.). Tracer measurements (Jones et al., 2008; Anderson et al., 2004) and model simulations (Karcher et al., 2006), on the other hand, suggest a change in the circulation of river water that was temporarily accumulating on the Siberian shelves and started to leave the shelves north of the East Siberian Sea around 1998. further east than previously. It subsequently replenished the 1990s LFW deficit in the central Arctic. This pulse of river water reached the Fram Strait in 2005, as observed by Rabe et al. (2009), and was also exported through the Canadian Arctic Archipelago. Observations have shown that the concentration of river water north of the Siberian Islands close to the Lomonosov Ridge was still higher in 2007 than in 1993 and 1995 (Abrahamsen et al., 2009), suggesting that also in the central Arctic the observed increases in LFW between the two time periods studied in this paper were caused by high concentrations of river water.

In summary, observations and the NAOSIM simulation indicate that the components of the changes in LFW vary by region: the shift in the LFW maximum in the Beaufort Gyre is likely a consequence of a mixture of changes in net sea ice melt, wind-ice stress induced EP and accumulation of advected river water. Around the Lomonosov Ridge, the Makarov Basin and in the Eurasian Basin the increase in river water from the Siberian shelves made the strongest contribution, whereas changes in the layer depth, although large, contributed much less. In addition, changes in layer depth in the Eurasian Basin could not be associated with EP during the 1990s in the simulation. Therefore, the freshening in the Eurasian Basin between the two time periods must have been caused by the properties and distribution of inflowing water and changes in the formation of the lower halocline. The product of changes in h and \bar{S} , represented by the last term in Equation 7 (Figure 4e), played a role only in small parts of the

331 Eurasian Basin (Figures 4c and d).

332 4.2 LFW content

333 On average over the whole domain, i.e. the upper deep Arctic Ocean, the depth of the 34 isohaline
334 increased by about 7 m effecting a volume increase of about 31000 km^3 , whereas the average salinity
335 above this isohaline decreased by about 0.5. Nevertheless, the thickness term in Equation 7 gives
336 an increase in LFWC by 1600 km^3 , whereas the salinity term results in $+6500 \text{ km}^3$. This means
337 that changes in \bar{S} contributed much more to changes in LFWC than changes in h ; therefore, EP
338 primarily redistributed LFW within the Arctic Ocean. The fact that the integral of the thickness-term
339 in Equation 7 over the whole deep Arctic Ocean is not zero may be explained by the regions where
340 the 34 isohaline is not in the adiabatic interior or where the 34 isohaline reached onto the shelves.
341 Furthermore, the thickness contribution is of the order of the uncertainty in the mapping process
342 (Appendix 7). On the other hand, decreases in \bar{S} originated from changes in ice formation and melt,
343 and inflow of LFW from the shelves. The non-linear term gives an increase of less than 300 km^3 and
344 is, therefore, negligible. Overall, the observed LFWC change is primarily due to changes in \bar{S} .

345 5 Summary and Conclusion

346 During July/August/September of 2006–2008 salinity profiles were measured across all Arctic Ocean
347 basins within a few years. These were used to analyze the distribution of LFW above the lower
348 halocline represented by the 34 isohaline. The measurements from 2006 – 2008 were compared to
349 observations from the 1990s, where measurements were more sparse but still covered most of the
350 deep Arctic Ocean.

- 351 1. The upper ocean LFW content for the deep Arctic Ocean during JAS increased by $8400 \pm$
352 2000 km^3 between 1992–1999 and 2006–2008. This is close to the annual export of freshwater
353 (liquid and solid) to and from the Arctic Ocean and almost 20 % of the average LFW content
354 observed for both time periods.
- 355 2. The spatial pattern of LFW changes simulated by NAOSIM agrees well with the observations

356 on large scales. The simulated LFW content change is, within the error margins, the same as
357 what was derived from observations.

358 3. Over the whole domain, changes in the observed depth of the 34 isohaline lead to a redistri-
359 bution of LFW and did not significantly influence the LFW content overall. In many regions,
360 the changes in the depth of the 34 isohaline lead to changes in LFW; in particular, north of the
361 Bering Strait, where the simulation suggests stronger anticyclonic stress during 2006 – 2008,
362 leading to a downward displacement of this isohaline due to downward Ekman pumping and
363 hence to an increase in LFW. Only in regions where the lower halocline is formed, north of the
364 Fram Strait and the Barents Sea, and north of the Canadian Arctic Archipelago, did we observe
365 diabatic changes in the depth of the 34 isohaline.

366 4. The observed LFW changes were largely due to a freshening of the layer above the 34 isohaline.
367 In the central Arctic, this was most likely due to enhanced advection of river water advected
368 from the shelves. In certain regions, such as north of the Bering Strait, increases in LFW can
369 be attributed to changes in the simulated net sea ice melt. In addition, the simulation shows
370 increases in net sea ice melt on the Siberian shelves that may have been advected into the
371 basins.

372 The observed change in the LFW content is equivalent to an average annual increase of about
373 750 km^3 between 1996 and 2007; the value in our simulation is about 550 km^3 . These values
374 are of similar magnitude as past changes seen in model studies by *Köberle and Gerdes (2007)* and
375 *Gerdes et al. (2008)*, where the LFW export from the Arctic Ocean between 1970 and 1995 was tem-
376 porarily enhanced by 500 km^3 annually, contributing to the LFWC decline in the Arctic over the same
377 period. River runoff has not changed on an Arctic-wide scale (*Serreze et al., 2006*). LFW transports
378 through the Bering Strait have been shown to vary on an interannual to multi-year timescale, but no
379 trend was observed between 1998 and 2008 (*Woodgate et al., 2006*, and pers. comm.). *Dmitrenko et al.*
380 (2008) have argued that, on average between 1920 and 2005, $500 \text{ km}^3/\text{yr}$ of LFW were advected from
381 the eastern Siberian shelf to the Arctic Ocean through the northeastern Laptev Sea during times of
382 anticyclonic atmospheric circulation. This value is again of similar order as the changes we observed.
383 Therefore, the most likely candidates for changing the LFWC between our two time periods are the
384 LFW exports from the Arctic to the Nordic Seas and the North Atlantic and the exchange between
385 the upper deep Arctic Ocean and the Siberian shelves.

Appendix

A Data processing procedures for salinity profiles

There are three categories of data we make use of in this study:

1. Data from ship CTDs directly obtained from the PIs only underwent a gross visual screening as these data were thoroughly processed and calibrated by the respective PIs and colleagues.
2. Data from WOD09 lying within our domain, the deep Arctic Ocean, only covers the first time period, 1992 – 1999. All data with a WOD flag of 1 (“outside range”) and 8 (“questionable data”) were discarded (please refer to the WOD09 manual for a description of ranges by region and depth interval; *Boyer et al.*, 2009). Furthermore, the data were thoroughly screened for spikes, unrealistic gradients and noise in the salinity profiles as well as gross offsets in temperature-salinity space. Any erroneous data were discarded or were replaced with data of better quality, where available. For example, the SCICEX93 (Scientific Ice Expeditions, 1993) data in WOD09 is in almost raw format, but those data are also available in a more advanced stage of processing, where SSXCTD casts from the submarine under the ice were corrected using surface CTD casts from the same expedition (*Morison et al.*, 1998).
3. Autonomous ice-based profilers, the WHOI Ice-tethered Profiler (ITP) and the MetOcean Polar Ocean Profiling System (POPS) provided a large number of profiles for 2006 – 2008. ITPs (*Krishfield et al.*, 2008) obtain profile data at about 0.25 m vertical resolution (1 Hz CTD sampling rate). These data were corrected for CTD sensor lags (*Johnson et al.*, 2007) and screened for erroneous data. Subsequently, a conductivity correction was performed by comparing the lower part of the profile with objectively mapped independently measured salinity on selected isotherms (potential temperatures {0.3, 0.4, 0.5}°C). After correction, the accuracy of the salinity data is 0.01. A detailed description of ITP processing procedures can be found in “ITP Data Processing Procedures” available at “<http://www.whoi.edu/itp/data/>”. POPS (*Kikuchi et al.*, 2007) provide data only at discrete pressure intervals, ranging from 2 dbar near the surface to 10 dbar in the lower part of the profile. Hence, sensor correction could not be applied to the POPS data, but data were thoroughly screened for errors. Subsequently, a conductivity correction was performed, using historical data as a reference in a similar way as for the ITPs. The

POPS vertical resolution is still above that of ARGO profilers, which claim an accuracy of 0.01 in salinity, after conductivity correction against historical data (*Owens and Wong, 2009*, and references therein). Therefore, we assume this accuracy also holds for data from POPS.

Any profiles that did not meet the following criteria were discarded: data gaps ranging over more than 20 *dbar* for either pressures lower than 150 *dbar* or salinities less than 34.5; more than 30 % of the data missing in the layer above the 34 isohaline. The remaining profiles were interpolated onto 2 *dbar* pressure levels, where interpolated values that were more than 3 *dbar* away from any original data point were eliminated. This avoids implausible interpolation across strongly stratified parts of the water column. Some duplicate profiles were manually identified and removed from the combined dataset. Further duplicates were eliminated in cases where more than one profile was found with the same latitude, longitude, time stamp and maximum profile pressure, within the following margins: two decimal places for latitude / longitude, six hours for time and 50 *dbar* for maximum profile pressure. Preference was given to profiles contained in datasets other than WOD09, if possible those obtained directly from the PIs responsible for their processing, as these data were of equal or better quality.

B Uncertainty in FWC estimates

The sources of error within our LFWC estimate consist of the statistical error associated with the mapping procedure, errors due to sampling gaps in regions of potentially high vertical gradients in salinity and errors due to the accuracy of the measurement devices.

The statistical mapping error is given at each grid point g by

$$\eta_g^2 = \langle s^2 \rangle - \omega \cdot C_{dg}^T + \frac{(1 - \omega)^2}{\sum (C_{dd} + I \cdot \langle \eta^2 \rangle)^{-1}}, \quad (8)$$

where the symbols are defined in Section 2.3.

We found η_g from mapping LFW to be highest ($> 1.5 m$) in regions without data, such as north of the Canadian Arctic Archipelago, but significant errors ($\sim 1 m$) were also found in regions of higher data coverage in the North American Basin due to uneven spatial distribution of the profiles and variability in the data (Figure 7). We tested the reliability of the LFWC estimate from the mapped

439 LFW inventories by considering only grid points below an error threshold: the difference in LFWC
440 between 2006 – 2008 and 1992 – 1999 considering only grid points with $\eta_g < 1.5 m$ is $8200 km^3$,
441 and using $\eta_g < 1 m$ it is $7600 km^3$; here, we use the field of combined error from both time periods,
442 considering the higher error of the two at each grid point. Considering only 1992 – 1999, the time
443 period with the higher mapping error, the estimate of the error is $2000 km^3$ using a threshold of
444 $< 1.5 m$, the same as that without a threshold, and $1800 km^3$ using a threshold of $< 1 m$. Hence,
445 our estimate of the difference in LFWC based on mapped LFW inventories appears to be robust with
446 respect to spatial coverage of the data. Furthermore, we performed the mapping with smaller distance
447 scales, L , (potential vorticity scales, Φ , were unchanged) and compared the resulting map to the one in
448 Figure 2c. Considering only grid points covered by both maps, we obtain a different LFWC for each
449 comparison: First, using $100 km$ and $50 km$ as the large and small distance scales, respectively, lead
450 to a difference in LFWC between both time periods of $5000 km^3$. This compares to $5100 km^3$ in the
451 mapping with scales of 600 and $300 km$. Second, mapping with $200/100 km$ leads to $7700 km^3$, which
452 is the same as the value from the $600/300 km$ map. The sensitivity of the LFWC difference between
453 the two time periods due to the fraction of randomly chosen data points in the mapping process is
454 around $100 km^3$. using five independent mappings of the same data in each time period. Likewise,
455 changing the reference salinity, S_{ref} , in Equation 1 to 34.8 only decreases the LFWC difference by
456 $200 km^3$. The sensitivity studies suggest that the difference in LFWC between both time periods is
457 between 6000 and $10000 km^3$

458 Data gaps in parts of the profile with strong vertical gradients of salinity near the surface may
459 introduce additional error to the LFW inventories and thus the LFWC. For example, autonomous
460 profilers, tethered to an ice floe, do not sample the top 7 to $10 m$; some other salinity profiles are
461 missing as much as the top $20 m$, the maximum allowed in our selection. We tested potential errors
462 in two ways:

- 463 1. A set of 215 CTD-based salinity profiles from two trans-Arctic Polarstern cruises, which took
464 stations in all the four Arctic Basins, is used. The LFW inventories using the full profiles,
465 usually starting at $2 dbar$, are compared to inventories using the value from $10 dbar$ in each
466 profile as a constant to the surface. In all 215 profiles, the maximum difference between the
467 salinity at $10 dbar$ and the minimum salinity in the layer to the surface is 2 , and only 12%
468 of these profiles show a salinity difference that leads to a difference in the LFW inventory of
469 more than $0.05 m$. This indicates that undersampling the upper $10 dbar$ leads to an error smaller

470 than that given by the mapping procedure. One caveat of this comparison is that during CTD
471 casts large research vessels evoke mixing of the upper 10 to 20 *m* due to the use of strong stern
472 or bow thrusters. While this does not affect vertically integrated quantities, such as our LFW
473 inventories, it may not fully resolve shallow layers of ice melt.

- 474 2. The LFW inventories were calculated assuming that the data was missing in a pressure interval
475 near the surface in all profiles. We did this calculation in two ways: First, we filled the artificial
476 gap by making a mixed layer assumption, using the shallowest data point below the gap for
477 constant extrapolation to the surface. Second, we did not fill the artificial gap, ignoring any
478 data within the pressure interval. Assuming a mixed layer in the pressure interval 0 to 10 *dbar*
479 or 0 to 20 *dbar*, the resulting LFWC differences between the two time periods are 8000 km^3
480 or 6800 km^3 , respectively. Even if we completely ignore the upper 10 *dbar* or 20 *dbar*, we
481 still obtain significant LFWC differences, 6700 km^3 or 4900 km^3 , respectively. Regardless of
482 how we treat any near-surface sampling gaps, the large scale patterns of the differences in LFW
483 inventories between the two time periods are similar to the one in Figure 2c, which is why the
484 corresponding maps are not shown here. Hence, the existence of near surface sampling gaps
485 does not alter our conclusion that a significant increase in LFWC occurred between 1992 – 1999
486 and 2006 – 2008.

487 Acknowledgments

488 We thank the participants of the various observational efforts listed in Table 1 for obtaining and
489 processing the salinity measurements. This work was supported by the Co-Operative Project “The
490 North Atlantic as Part of the Earth System: From System Comprehension to Analysis of Regional
491 Impacts” funded by the German Federal Ministry for Education and Research (BMBF) and by the Eu-
492 ropean Union Sixth Framework Programme project DAMOCLES (Developing Arctic Modelling and
493 Observing Capabilities for Long-term Environment Studies), contract number 018509GOCE. This
494 work is a contribution to the “Helmholtz Climate Initiative REKLIM” (Regional Climate Change), a
495 joint research project by the Helmholtz Association of German research centres (HGF).

References

- 496
- 497 Aagaard, K., and E. C. Carmack (1989), The role of sea ice and other fresh water in the Arctic
498 circulation, *J. Geophys. Res.*, *94*(C10), 14,485–14,498.
- 499 Abrahamsen, E. P., M. P. Meredith, K. K. Falkner, S. Torres-Valdes, M. J. Leng, M. B. Alkire, S. Ba-
500 con, S. W. Laxon, I. Polyakov, and V. Ivanov (2009), Tracer-derived freshwater composition of the
501 Siberian continental shelf and slope following the extreme Arctic summer of 2007, *Geophys. Res.*
502 *Let.*, *36*, L07602, doi:10.1029/2009GL037341.
- 503 Anderson, L. G., S. Jutterström, S. Kaltin, E. P. Jones, and G. Björk (2004), Variability in river
504 runoff distribution in the Eurasian Basin of the Arctic Ocean, *J. Geophys. Res.*, *109*, doi:10.1029/
505 2003JC001773.
- 506 Böhme, L., and U. Send (2005), Objective analyses of hydrographic data for referencing profiling
507 float salinities in highly variable environments, *Deep-Sea Res. II*, *52*(3-4), 651–664, doi:10.1016/j.
508 dsr2.2004.12.014.
- 509 Böhme, L., M. P. Meredith, S. E. Thorpe, M. Biuw, and M. Fedak (2008), The ACC frontal system in
510 the South Atlantic: monitoring using merged Argo and animal-borne sensor data, *J. Geophys. Res.*,
511 *113*, C09012, doi:10.1029/2007JC004647.
- 512 Boyer, T., J. I. Antonov, O. K. Baranova, H. E. Garcia, D. R. Johnson, R. A. Locarnini, A. V. Mis-
513 honov, T. D. O'Brien, D. Seidov, I. V. Smolyar, and M. M. Zweng (2009), World ocean database
514 2009, in *NOAA Atlas NESDIS*, vol. 66, edited by S. Levitus, U.S. Government Printing Office,
515 Washington, D.C., 216 pp, DVDs.
- 516 Brauch, J. P., and R. Gerdes (2005), Reaction of the northern North Atlantic and Arctic oceans to a
517 sudden change of the NAO, *J. Geophys. Res.*, *110*, C11018, doi:10.1029/2004JC002436.
- 518 Bretherton, F. P., R. E. Davis, and C. B. Fandry (1976), A technique for objective analysis and design
519 of oceanographic experiments applied to MODE-73, *Deep-Sea Res. I*, *23*, 559–582.
- 520 Curry, R., and C. Mauritzen (2005), Dilution of the Northern North Atlantic Ocean in Recent Decades,
521 *Science*, *308*, 1772–1774, doi:10.1126/science.1109477.
- 522 Davis, R. E. (1998), Preliminary results from directly measuring middepth circulation in the tropical
523 and South Pacific, *J. Geophys. Res.*, *103*(C11), 24,619–24,639.
- 524 de Steur, L., E. Hansen, R. Gerdes, E. Karcher, M. anFahrbach, and J. Holfort (2009), Freshwater
525 fluxes in the East Greenland Current: A decade of observations, *Geophys. Res. Let.*, *36*, L23611,
526 doi:10.1029/2009GL041278.

- 527 Dickson, R., B. Rudels, S. Dye, M. Karcher, J. Meincke, and I. Yashayaev (2007), Current estimates
528 of freshwater flux through Arctic and subarctic seas, *Progress in Oceanography*, 73, 210–230,
529 doi:10.1016/j.pocean.2006.12.003.
- 530 Dmitrenko, I. A., S. A. Kirillov, and L. B. Tremblay (2008), The long-term and interannual variability
531 of summer fresh water storage over the eastern Siberian shelf: Implication for climatic change, *J.*
532 *Geophys. Res.*, 113, C03007, doi:10.1029/2007JC004304.
- 533 Dukhovskoy, D. S., M. A. Johnson, and A. Proshutinsky (2004), Arctic decadal variability: An auto-
534 oscillatory system of heat and fresh water exchange, *Geophys. Res. Lett.*, 31, L03302, doi:10.1029/
535 2003GL019023.
- 536 Gerdes, R., M. Karcher, C. Köberle, and K. Fieg (2008), Simulating the long term variability of liquid
537 freshwater export from the Arctic Ocean, in *Arctic-Subarctic Ocean Fluxes: Defining the role of*
538 *the Northern Seas in climate*, edited by R. R. Dickson, J. Meincke, and P. Rhines, chap. 17, pp.
539 405–425, Springer Science and Business Media.
- 540 Haak, H., U. Jungclauss, U. Mikolajewicz, and M. Latif (2003), Formation and propagation of great
541 salinity anomalies, *Geophys. Res. Lett.*, 30, 1473, doi:10.1029/2003GL01765.
- 542 Häkkinen, S. (1999), A simulation of the thermohaline effects of a great salinity anomaly, *J. Climate*,
543 12, 1781–1795.
- 544 Häkkinen, S., and A. Proshutinsky (2004), Freshwater content variability in the Arctic Ocean, *J.*
545 *Geophys. Res.*, 109, C03051, doi:10.1029/2003JC001940.
- 546 Holbrook, N. J., and N. L. Bindoff (2000), A statistically efficient mapping technique for four-
547 dimensional ocean temperature data, *Journal of Atmospheric and Oceanic Technology*, 17(6),
548 831846.
- 549 Itoh, M., and K. Shimada (2003), XCTD salinity calibration in the Arctic Ocean, *Tech. Rep. 48*,
550 Report of Japan Marine Science and Technology Center (JAMSTEC-R), JAMSTEC, Yokosuka,
551 Japan.
- 552 Jakobsson, M., R. Macnab, M. Mayer, R. Anderson, J. Edwards, M. and Hatzky, H.-W. Schenke,
553 and P. Johnson (2008), An improved bathymetric portrayal of the Arctic Ocean: Implications for
554 ocean modeling and geological, geophysical and oceanographic analyses, *Geophys. Res. Lett.*, 35,
555 doi:10.1029/2008GL033520.
- 556 Johnson, G. C., J. M. Toole, and N. G. Lason (2007), Sensor Corrections for Sea-Bird SBE-41CP and
557 SBE-41 CTDs, *J. Atmos. Ocean. Technol.*, 24(6), 1117–1130, doi:DOI:10.1175/JTECH2016.1.

- 558 Jones, E. P., L. G. Anderson, S. Jutterström, L. Mintrop, and J. H. Swift (2008), Pacific fresh water,
559 river water and sea ice meltwater across Arctic Ocean basins: Results from the 2005 Beringia
560 Expedition, *J. Geophys. Res.*, *113*, C08012, doi:10.1029/2007JC004124.
- 561 Kalnay, E., and coworkers (1996), The NCEP/NCAR 40-Year Reanalysis Project, *Bull. Am. Meteorol.*
562 *Soc.*, *77*(3), 437–495.
- 563 Karcher, M., R. Gerdes, F. Kauker, C. Köberle, and I. Yashayaev (2005), Arctic Ocean change heralds
564 North Atlantic freshening, *Geophys. Res. Lett.*, *32*, doi:10.1029/2005GL023861.
- 565 Karcher, M., R. Gerdes, and F. Kauker (2006), Modeling of $\delta_{18}\text{O}$ and ^{99}Tc dispersion in Arctic and
566 subarctic seas, *ASOF Newsletter*, *5*, available from: <http://asof.npolar.no>.
- 567 Karcher, M. J., R. Gerdes, F. Kauker, and C. Köberle (2003), Arctic warming: Evolution and spread-
568 ing of the 1990s warm event in the Nordic seas and the Arctic Ocean, *J. Geophys. Res.*, *108*(C2),
569 doi:doi10.1029/2001JC001265.
- 570 Kauker, F., R. Gerdes, M. Karcher, C. Köberle, and J. L. Lieser (2003), Variability of Arctic and
571 North Atlantic sea ice: A combined analysis of model results and observations from 1978 to 2001,
572 *J. Geophys. Res.*, *108*(C6), doi:doi10.1029/2002JC001573.
- 573 Kikuchi, T. (2008), XCTD observation, in *The Expedition ARKTIS-XXII/2 of the Research Vessel*
574 *“Polarstern” in 2007, Reports on polar and marine research*, vol. 579, edited by U. Schauer, pp.
575 96–102, Alfred-Wegener Institute for Polar and Marine Research: Bremerhaven, Germany.
- 576 Kikuchi, T., J. Inoue, and D. Langevin (2007), Argo-type profiling float observations under the Arctic
577 multiyear ice, *Deep-Sea Res. I*, *54*(9), 1675–1686.
- 578 Köberle, C., and R. Gerdes (2003), Mechanisms determining the variability of Arctic sea ice condi-
579 tions and export, *J. Climate*, *16*, 2843–2858.
- 580 Köberle, C., and R. Gerdes (2007), Simulated variability of the Arctic Ocean fresh water balance
581 1948-2001, *J. Phys. Oceanogr.*, *37*, 1628–1644, doi:10.1175/JPO03063.1.
- 582 Koenigk, T., U. Mikolajewicz, H. Haak, and J. Jungclaus (2007), Arctic freshwater export in the 20th
583 and 21st centuries, *J. Geophys. Res.*, *112*, G04S41, doi:10.1029/2006JG000274.
- 584 Krishfield, R., J. Toole, A. Proshutinsky, and M. L. Timmermans (2008), Automated Ice-Tethered
585 Profilers for seawater observations under pack ice in all seasons, *J. Atmos. Oceanic Tehnol.*, *25*,
586 2091–2105.
- 587 MacDonald, R. W. (2000), Arctic estuaries and ice: a positive-negative estuarine couple, in *The*
588 *freshwater budget of the Arctic Ocean, NATO Science Partnership Sub-Series: 2*, vol. 70, edited by

- 589 E. L. Lewis, E. P. Jones, P. Lemke, T. D. Prowse, and P. Wadhams, pp. 383–407, Kluwer Academic:
590 Netherlands.
- 591 McIntosh, P. C. (1990), Oceanographic data interpolation: objective analysis and splines, *J. Geophys.*
592 *Res.*, 95(C8), 13,529.
- 593 Morison, J., M. Steele, T. Kikuchi, K. Falkner, and W. Smethie (2006), Relaxation of central
594 Arctic Ocean hydrography to pre-1990s climatology, *Geophys. Res. Lett.*, 33, L17604, doi:
595 10.1029/2006GL026826.
- 596 Morison, J. H., M. Steele, and R. Andersen (1998), Hydrography of the upper Arctic Ocean measured
597 from the nuclear submarine USS Pargo, *Deep-Sea Res. I*, 45, 15–38.
- 598 Newton, R., P. Schlosser, D. G. Martinson, and W. Maslowski (2008), Freshwater distribution in the
599 Arctic Ocean: simulation with a high resolution model and model-data comparison, *J. Geophys.*
600 *Res.*, 113, C05024, doi:10.1029/2007JC004111.
- 601 Owens, W. B., and A. Wong (2009), An improved calibration method for the drift of the conductivity
602 sensor on autonomous CTD profiling floats by -S climatology, *Deep-Sea Res. I*, 56(3), 450.
- 603 Pacanowski, R. C. (1995), MOM 2 Documentation, users guide and reference manual, *GFDL Ocean*
604 *Group Tech. Rep. 3*, Geophys. Fluid Dyn. Lab., Princeton Univ., Princeton, N. J.
- 605 Polyakov, I. V., V. Alexeev, F. I. Belchansky, I. A. Dmitrenko, V. Ivanov, S. Kirillov, A. Korablev,
606 M. Steele, L. A. Timokhov, and I. Yashayaev (2008), Arctic Ocean freshwater changes over the
607 past 100 year and their causes, *J. Climate*, 21(2).
- 608 Proshutinsky, A. Y., and M. A. Johnson (1997), Two circulation regimes of the wind-driven Arctic
609 Ocean, *J. Geophys. Res.*, 102, 12,493–12,514.
- 610 Proshutinsky, A., R. Krishfield, M.-L. Timmermans, J. Toole, E. Carmack, F. McLaughlin, W. J.
611 Williams, S. Zimmermann, M. Itoh, and K. Shimada (2009), Beaufort Gyre freshwater reservoir:
612 State and variability from observation, *J. Geophys. Res.*, 114, doi:10.1029/2008JC005104.
- 613 Rabe, B., A. Mackensen, U. Schauer, M. Karcher, E. Hansen, and A. Beszczynska-Möller (2009),
614 Freshwater components and transports in the FRAM Strait: Recent observations and changes since
615 the late 1990s, *Ocean Sci.*, 5, 219–233, doi:10.5194/os-5-219-2009.
- 616 Rennermalm, A. K., E. F. Wood, A. J. Weaver, M. Eby, and S. J. Derý (2007), Relative sensitivity of
617 the Atlantic meridional overturning circulation to river discharge into Hudson Bay and the Arctic
618 Ocean, *J. Geophys. Res.*, 112, G04S45, doi:10.1029/2006JG000330.
- 619 Rudels, R., E. P. Jones, U. Schauer, and P. Ericksson (2004), Atlantic sources of the Arctic Ocean

- 620 surface and halocline waters, *Polar Research*, 23(2), 181–208.
- 621 Schauer, U., E. Fahrbach, S. Østerhus, and G. Rohardt (2004), Arctic warming through the Fram
622 Strait: Oceanic heat transport from 3 years of measurements, *J. Geophys. Res.*, 109, doi:10.1029/
623 2003JC001823.
- 624 Serreze, M. C., a. P. Barrett, A. G. Slater, R. Woodgate, K. Aagaard, R. B. Lammers, M. Steele,
625 R. Moritz, M. Meredith, and C. M. Less (2006), The large-scale freshwater cycle of the Arctic, *J.*
626 *Geophys. Res.*, 111(C11), doi:10.1029/2005JC003424.
- 627 Steele, M., and T. Boyd (1998), Retreat of the cold halocline layer in the Arctic Ocean, *J. Geophys.*
628 *Res.*, 103(C5), 10,419–10,439.
- 629 Steele, M., R. Morley, and W. Ermold (2001), PHC: A global ocean hydrography with a high quality
630 Arctic Ocean, *J. Climate*, 14, 2079–2087.
- 631 Steele, M., J. Morison, W. Ermold, I. Rigor, M. Ortmeyer, and K. Shimada (2004), Circulation
632 of summer Pacific halocline water in the Arctic Ocean, *J. Geophys. Res.*, 109, doi:doi10.1029/
633 2003JC002009.
- 634 Stevens, D. P. (1991), On open boundary condition in the United Kingdom 979 Fine-Resolution
635 Antarctic Model, *J. Phys. Oceanogr.*, 21, 1494–1499.
- 636 Woodgate, R. A., K. Aagaard, and T. J. Weingartner (2006), Interannual changes in the Bering Strait
637 fluxes of volume, heat and freshwater between 1991 and 2004, *Geophys. Res. Lett.*, 33, doi:10.
638 1029/2006GL026931.
- 639 Yamamoto-Kawai, M., F. A. McLaughlin, E. C. Carmack, S. Nishino, K. Shimada, and N. Kurita
640 (2009), Surface freshening of the Canada Basin, 2003-2007: River runoff versus sea ice meltwater,
641 *J. Geophys. Res.*, 114, C00A05, doi:10.1029/2008JC005000.
- 642 Yang, J. (2006), The seasonal variability of the Arctic Ocean Ekman transport and its role in the mixed
643 layer heat and salt fluxes, *J. Climate*, 19, 5366–5387.

644 **T**ables and figures

645

646

| Expedition, project or institute | Year(s) | Platform | Source URL or contact |
|---|----------------------|---------------|---|
| World Ocean Database 2009 | 1992 – 1999 | various | http://www.nodc.noaa.gov/OC5/WOD09 |
| Scientific Ice Exercises (SCICEX) | 1993 | US submarines | http://data.eol.ucar.edu/codiac/dss/id=106.arcss072/ |
| ARK IX/4 | 1993 | RV Polarstern | http://www.pangaea.de/ |
| ARK XI | 1995 | RV Polarstern | http://www.pangaea.de/ |
| ARK XII | 1996 | RV Polarstern | http://www.pangaea.de/ |
| Scientific Ice Exercises (SCICEX) | 1996, 1997 and 1998, | US submarines | SAIC project, Sergey Pisarev (pisarev@ocean.ru) |
| ARK XIII | 1997 | RV Polarstern | http://www.pangaea.de/ |
| Scientific Ice Exercises (SCICEX) | 1997 and 1998, | US submarines | http://data.eol.ucar.edu/codiac/dss/id=106.arcss064/ |
| ARK XV | 1999 | RV Polarstern | http://www.pangaea.de/ |
| Beaufort Gyre Project | 2006 – 2008 | various ships | http://www.whoi.edu/beaufortgyre/ |
| European Union project DAMOCLES | 2006 – 2008 | POPS | http://www.ipev.fr/damocles/ |
| ARGO | 2006 – 2008 | POPS | http://www.coriolis.eu.org/cdc/argo.htm |
| Woods Hole Oceanographic Institution (WHOI) | 2006 – 2008 | ITP | http://www.whoi.edu/itp |
| ARK XXII/2 (SPACE) | 2007 | RV Polarstern | http://www.pangaea.de/ |
| LOMROG 2007 | 2007 | RV Oden | Göran Björk (gobj@gvc.gu.se) |
| Nansen / Amundsen Basins Observ. System (NABOS) | 2007, 2008 | various ships | http://nabos.iarc.uaf.edu/ |
| ARK XXIII/3 (AMEX I) | 2008 | RV Polarstern | http://www.pangaea.de/ |
| Arctic Summer Cloud Ocean Study (ASCOS) | 2008 | RV Oden | http://www.ascos.se (Anders Sirevaag) |

Table 1: Data sources for salinity observations during JAS. The autonomous measurements were undertaken using the Ice-Tethered Profiler (ITP) and the Polar Ocean Profiling System (POPS). Data taken from the online World Ocean Database 2009 (WOD09; *Boyer et al.*, 2009) were used to augment but not replace profiles from the other datasets listed in the table. SCICEX data from the SAIC project were used, where available, to replace profiles from the 1997 and 1998 SCICEX expeditions downloadable from EOL. The SCICEX 1993 data from EOL were preferred over those from SAIC due to more advanced processing.

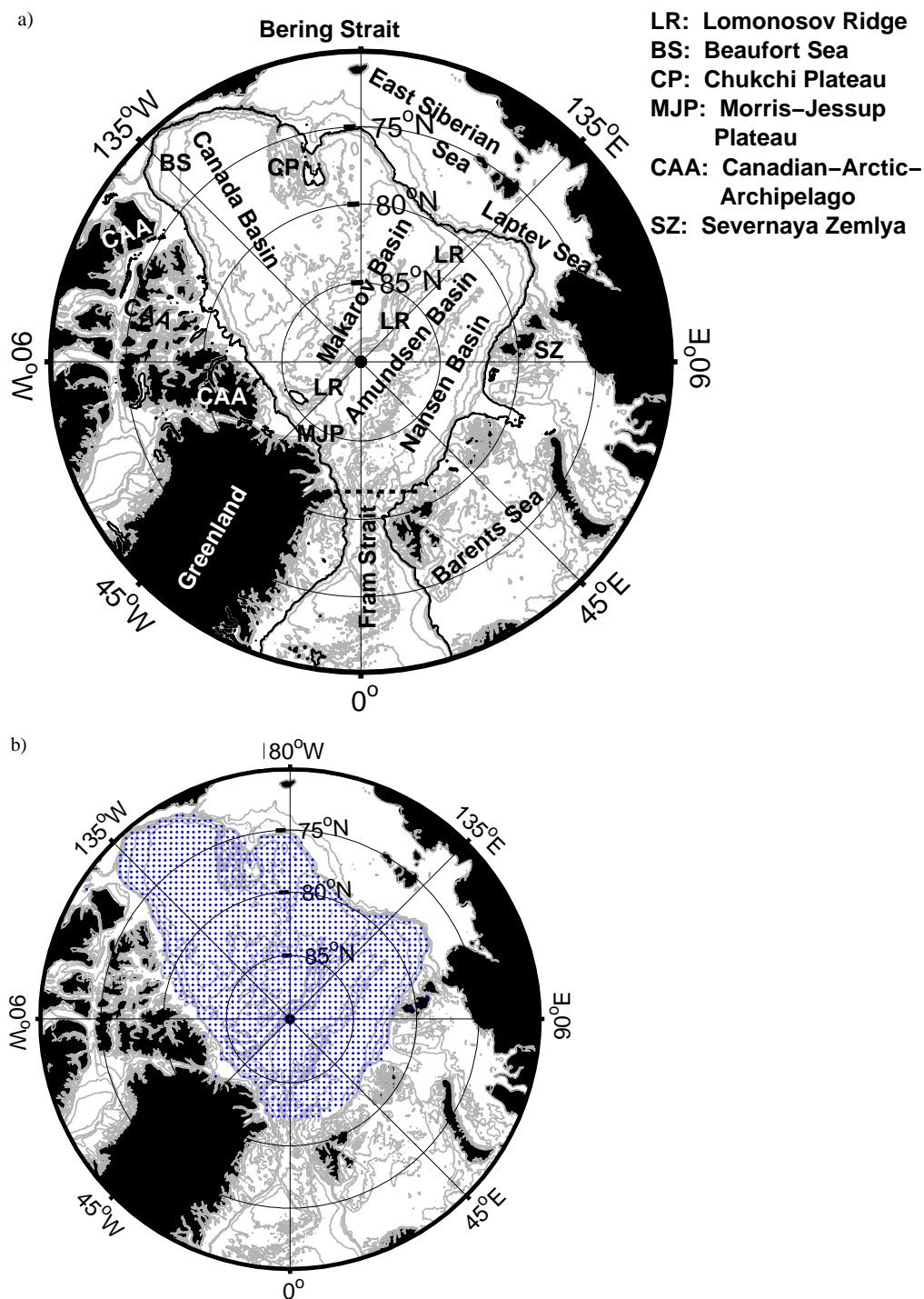


Figure 1: Bathymetry of the Arctic Ocean from the IBCAO database (IBCAO Jakobsson *et al.*, 2008): (a) geographic names; gray contour lines represent the bathymetric depths 100, 200, 500, 750, 1000, 2000, 3000 and 4000 *m*. The 500 *m* isobath represents the boundary of our “deep Arctic Ocean” domain and is shown as a thick black line; additionally, the domain was restricted to north of 82°N north of the Fram Strait (dashed line). Whenever we refer to the “North American Basin” and the “Eurasian Basin” it incorporates the Makarov and Canada basins and the Amundsen and Nansen basins, respectively. (b) Grid used for objective mapping.

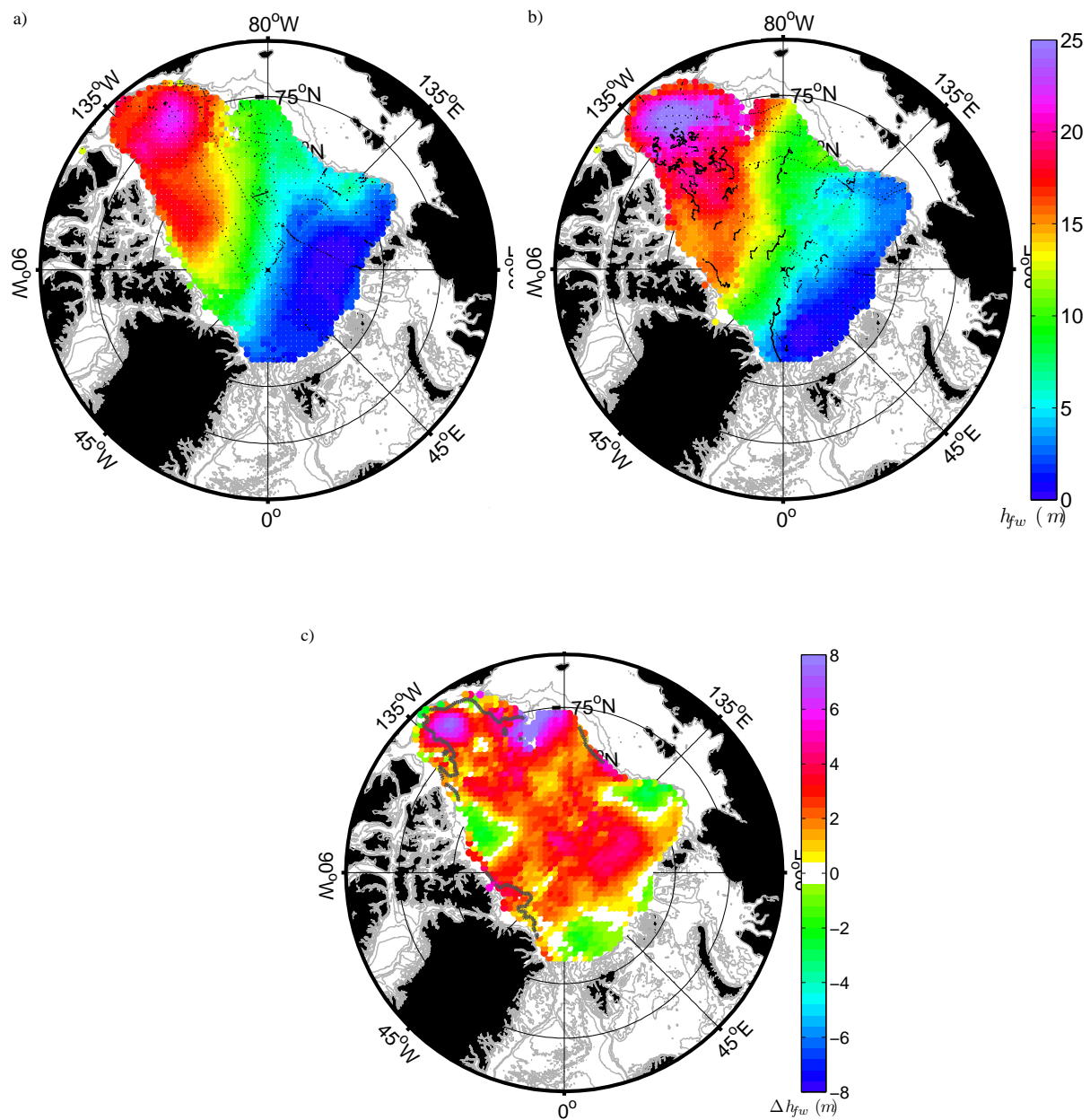


Figure 2: Objectively mapped observed freshwater inventory from the surface to the depth of the 34 isohaline for the deep Arctic Ocean during JAS: (a) 1992 – 1999 and (b) 2006 – 2008. The anomaly of 2006 – 2008 relative to 1992 – 1999 is shown in (c). The locations of measured salinity profiles used for the mapping are shown as black dots in (a) and (b); larger dots are shown in Figure 7. Only (c): values within ± 0.25 m of zero are white; the thick gray line represent the 1 m contour of the combined (maximum) statistical error estimate for both mapping time periods (see Figure 7).

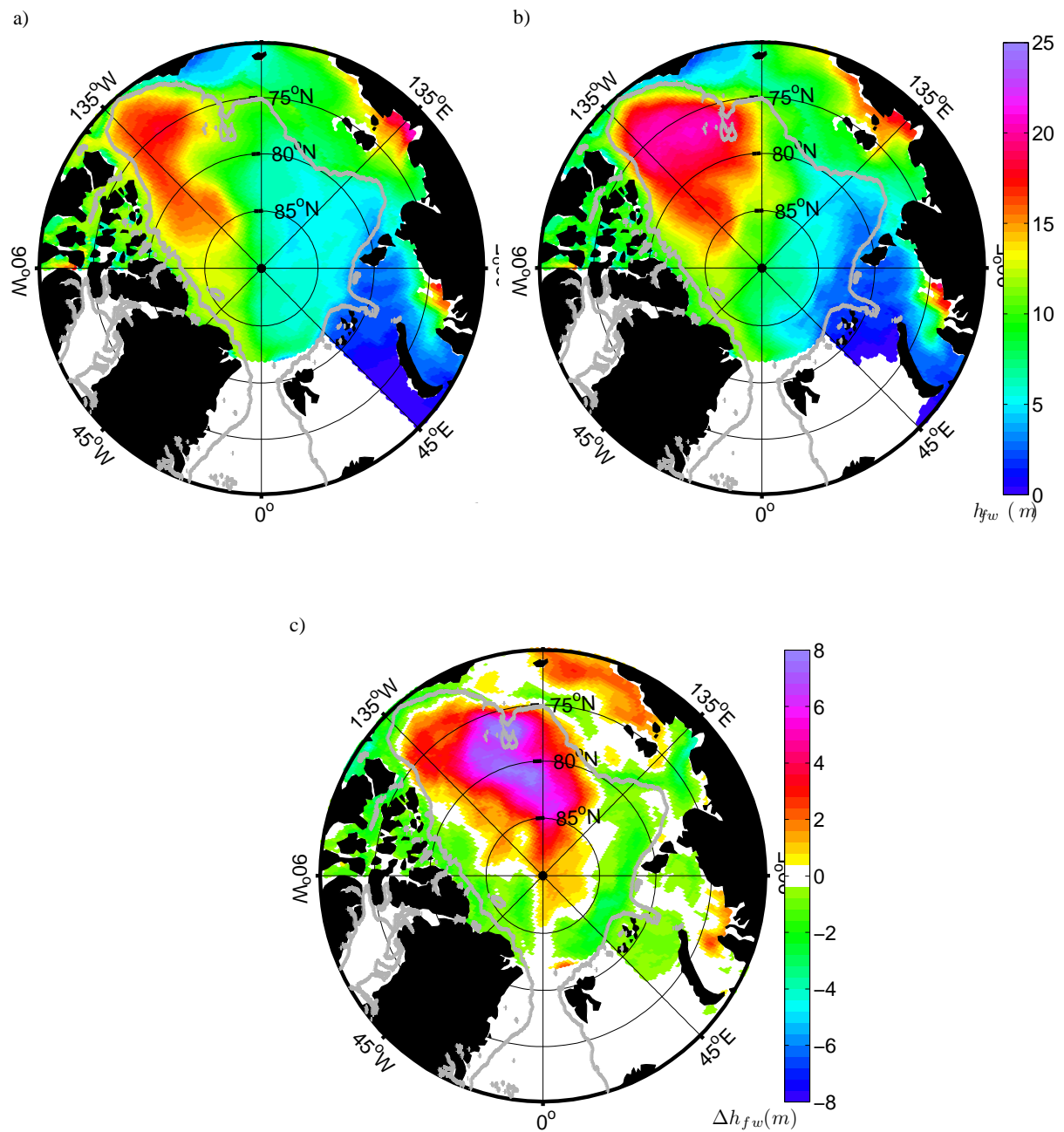


Figure 3: Time averages of freshwater inventories from the surface to the depth of the 34 isohaline in the NAOSIM simulation during JAS for the time periods (a) 1992 – 1999 and (b) 2006 – 2008, and (c) the anomaly of 2006 – 2008 relative to 1992 – 1999. The thick gray line represents the 500 m isobath (IBCAO bathymetry), and the region south of 82°N in the Fram Strait is left blank, as it is not considered in the analysis.

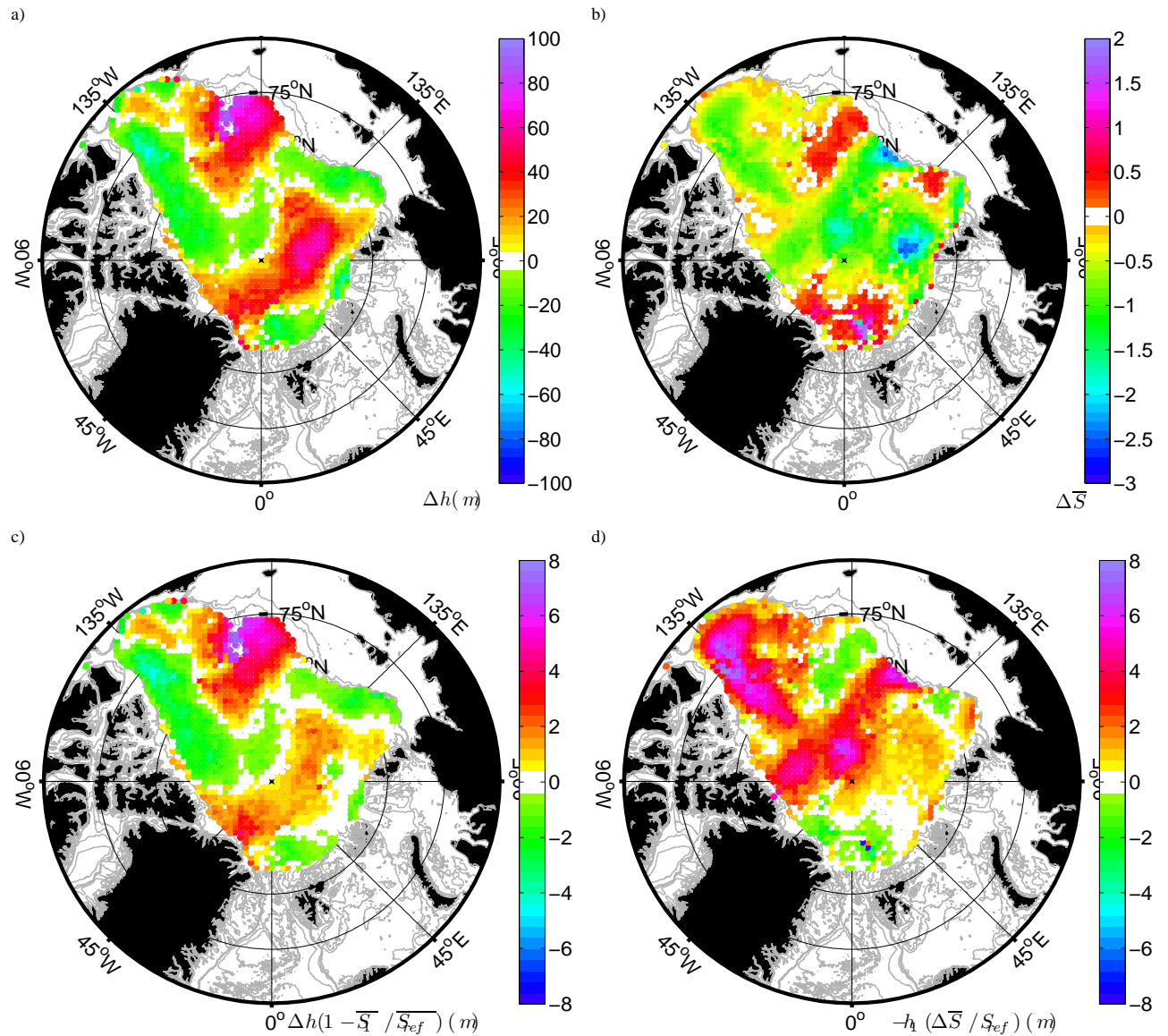


Figure 4: Difference between 2006 – 2008 and 1992 – 1999 from observations in the deep Arctic Ocean during JAS of (a) the depth of the 34 isohaline, $h = z(S = 34)$, and (b) the mean salinity above the 34 isohaline. (c), (d) and (e) show the “thickness”, “salinity” and “non-linear” terms in Equation 7, respectively. Values within ± 0.25 m (a and c to e) or ± 0.125 (b) of zero are white.

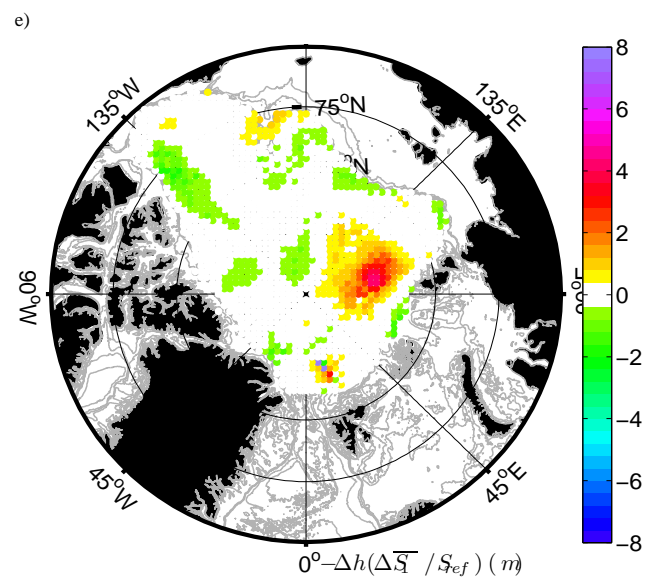


Figure 4: continued...

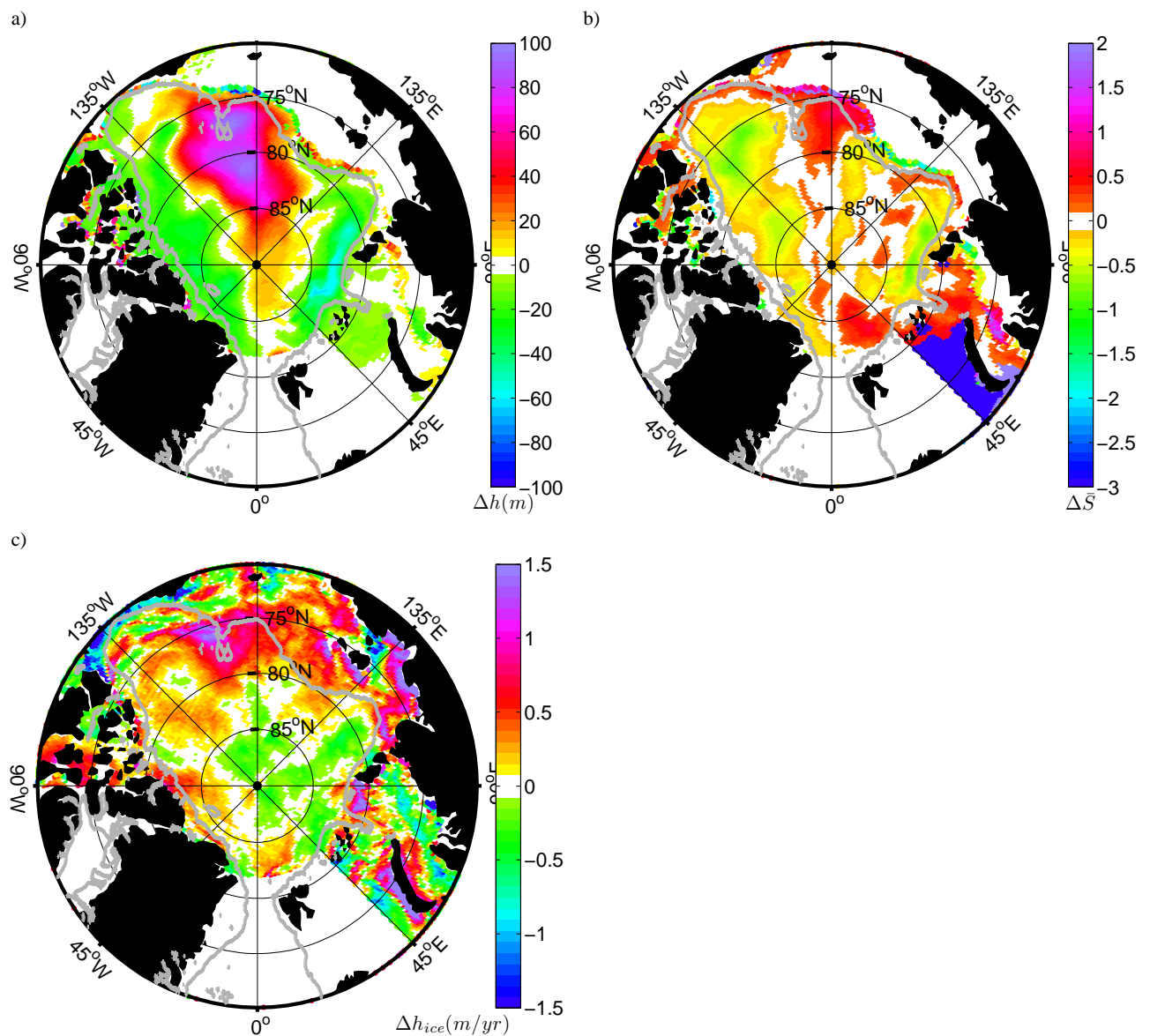


Figure 5: Difference in time averages from the NAOSIM simulation between the time periods 2006 – 2008 and 1992 – 1999: (a) depth of the 34 isohaline (JAS), (b) depth-averaged salinity above this isohaline (JAS), and (c) the net sea ice melt (all year). Positive values in (d) represent a reduction in thermodynamic sea ice growth or an increase in sea ice melt. The 500 *m* isobath (IBCAO bathymetry) is shown as a thick gray line, and the region south of 82° *N* in the Fram Strait is left blank, as it is not considered in the analysis.

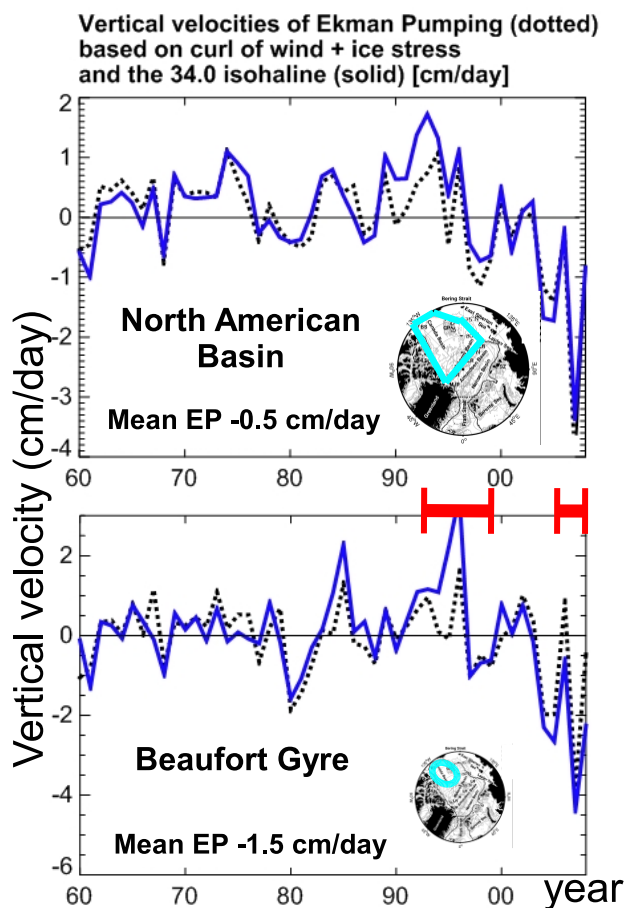


Figure 6: Time series of annual mean vertical velocity (positive upward) in the NAOSIM simulation derived from Ekman Pumping (EP; dotted), based on the curl of the ocean-surface (wind and ice) stress, and from the vertical displacement of the 34.0 isohaline (solid). Shown is the spatial means for the North American Basin and the Beaufort Gyre, where the EP velocity is offset by the time mean for each region. The regions used for spatial averaging are sketched in the inlaid maps, and the x-axis shows the time from 1960 until 2008 (middle-of-year), where the two time periods under study in our FW analysis are marked as red horizontal bars.

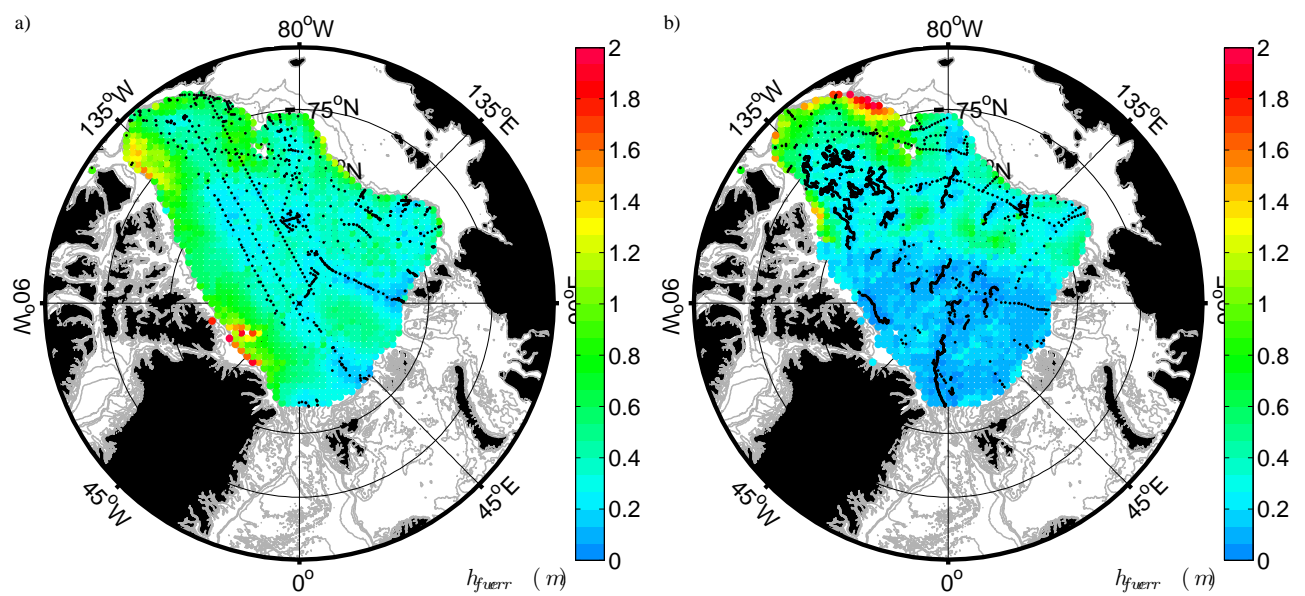


Figure 7: Statistical error estimate (Equation 8) associated with the objective maps of freshwater inventories in Figure 2: (a) 1992 – 1999 and (b) 2006 – 2008. The locations of measured salinity profiles used for the mapping are shown as black dots.